

# Exploring atom-ion Feshbach resonances below the $s$ -wave limit

Fabian Thielemann,<sup>1</sup> Joachim Siemund,<sup>1</sup> Daniel von Schoenfeld,<sup>1</sup> Wei Wu,<sup>1,2</sup> Pascal Weckesser,<sup>1,3,4</sup> Krzysztof Jachymski,<sup>5</sup> Thomas Walker,<sup>1,2,6</sup> and Tobias Schaetz<sup>1,2</sup>

<sup>1</sup>*Physikalisches Institut, Albert-Ludwigs-Universität Freiburg,  
Hermann-Herder Str. 3, 79104 Freiburg, Germany*

<sup>2</sup>*EUCOR Centre for Quantum Science and Quantum Computing,  
Albert-Ludwigs-Universität Freiburg, 79104 Freiburg, Germany*

<sup>3</sup>*Max-Planck-Institut für Quantenoptik, 85748 Garching, Germany*

<sup>4</sup>*Munich Center for Quantum Science and Technology (MCQST), 80799 Munich, Germany*

<sup>5</sup>*Faculty of Physics, University of Warsaw, Pasteura 5, 02-093 Warsaw, Poland*

<sup>6</sup>*Blackett Laboratory, Imperial College London,  
Prince Consort Road, London SW7 2AZ, United Kingdom*

(Dated: June 21, 2024)

## Abstract

Revealing the quantum properties of matter requires a high degree of experimental control accompanied by a profound theoretical understanding. At ultracold temperatures, quantities that appear continuous in everyday life, such as the motional angular momentum of two colliding particles, become quantized, leaving a measurable imprint on experimental results. Embedding a single particle within a larger quantum bath at lowest temperatures can result in resonant partial-wave dependent interaction, whose strength near zero energy is dictated by universal threshold laws. Hybrid atom-ion systems have emerged as a novel platform in which a single charged atom in an ultracold bath serves as a well-controlled impurity of variable energy. However, entering the low-energy  $s$ -wave regime and exploring the role of higher-partial wave scattering within has remained an open challenge. Here, we immerse a Barium ion in a cloud of ultracold spin-polarized Lithium atoms, realize tunable collision energies below the  $s$ -wave limit and explore resonant higher-partial wave scattering by studying the energy-dependence of Feshbach resonances. Utilizing precise electric field control, we tune the collision energy over four orders of magnitude, reaching from the many-partial-wave to the  $s$ -wave regime. At the lowest energies, we probe the energy-dependence of an isolated  $s$ -wave Feshbach resonance and introduce a theoretical model that allows to distinguish it from higher-partial-wave resonances. Additionally, at energies around the  $p$ -wave barrier, we find and identify an open-channel  $f$ -wave resonance, consistent with threshold laws. Our findings highlight and benchmark the importance of higher-partial wave scattering well within the  $s$ -wave regime and offer control over chemical reactions and complex many-body dynamics in atom-ion ensembles – on the level of individual angular momentum quanta.

## I. INTRODUCTION

Resonant scattering is of major importance in a variety of physical processes, ranging from particle creation to photons interacting with optical cavities. At the lowest temperatures, where particles exhibit wave-like behavior, interference effects can drastically alter the outcome of a collision [1]. The transition into this regime is typically marked by reaching collision energies below the  $s$ -wave limit; that is the energetic height of the lowest collisional angular momentum barrier ( $\ell = 1$ ). For most neutral gases the  $s$ -wave limit is well above the Doppler temperature, facilitating the access to Feshbach resonances that fuel the ongoing investigation of various many-particle Hamiltonians or the interaction between atoms at close range [2, 3]. Near a Feshbach resonance, external magnetic fields can be used to vary the atomic interaction from attractive to repulsive or even tune it out entirely – experimentally evidenced by monitoring the loss of colliding particles from the trap. Studying Feshbach resonances in various energy regimes can reveal the physical laws behind the involved loss processes. This has been used to demonstrate how Pauli’s exclusion principle suppresses the  $s$ -wave scattering of ultracold spin-polarized fermions [4], to understand the chaotic Feshbach resonance spectra of Lanthanides [5], or to study a novel resonant loss process in ultracold molecular collisions [6]. These studies of neutral gases are typically constrained to energies below the  $p$ -wave barrier by the finite depth of optical traps. On the other hand, merged beam experiments with precise control over collision energies of a few millikelvin and above have unveiled intricate details of quantum resonant loss processes like the role of Feshbach resonance pathways on the final state distribution [7, 8]. Applying similar methods to novel platforms, such as atom-ion systems in the ultracold regime, is particularly interesting.

An ion, embedded in an ultracold atomic gas, is an intriguing system to study collision energy effects at ultracold temperatures: the ion serves as a single, highly controllable probe and interacts with the atoms via the long-range isotropic charge-induced-dipole interaction, allowing novel applications ranging from quantum simulations to cold chemistry [9–12]. However, the  $1/R^4$  scaling (where  $R$  is the distance between ion and atom) at long range implies that much lower collision energies are required to enter the  $s$ -wave regime. As an example, the  $s$ -wave limit for Li-Ba<sup>+</sup> is  $E_s = 8.8 \mu\text{K}$ , in contrast to the orders of magnitude larger  $E_{s,\text{Li-Li}} \approx 8 \text{ mK}$  in the case of Li-Li collisions, a workhorse in the field of ultracold atom experiments. In fact, the few-partial wave regime has only recently been reached, as experimentally witnessed by a variation of the spin-exchange rate in  ${}^6\text{Li-}^{171}\text{Yb}^+$  and the direct observation of Feshbach resonances in  ${}^6\text{Li-}^{138}\text{Ba}^+$  [13, 14]. In the latter case with Li polarized in the second lowest hyperfine state, 13 resonances were discovered within a range of approximately 100 G, substantially more than in most alkali atom-atom combinations. The unusually high density

of Feshbach resonances is in part due to overlap between the singlet and triplet ground states of the  $\text{LiBa}^+$  molecule with its electronically excited  $b^3\Pi$  state that lead to significant second-order spin-orbit interaction and allow coupling between different total spin channels. This additional coupling turned out to add considerable complexity to numerical calculations [14, 15]. An experimental investigation of the energy dependence of individual Feshbach resonances could provide the missing ingredient for numerical calculations. So far, studying the energy dependence of inelastic atom-ion collisions in the many-partial-wave regime shed light on three-body recombination processes [16, 17]. Extending this control to energies below  $E_s$  could reveal the microscopic properties of atom-ion Feshbach resonances, such as their partial-wave assignment, and allow for a new level of control over complex many-body dynamics at ultracold temperatures.

In this Article, we demonstrate collision energy tuning below the atom-ion  $s$ -wave limit  $E_s$  and apply our method to assign the partial-wave order of selected Feshbach resonances. Preparing the atoms in their hyperfine ground state and the ion at lowest kinetic energy, we find a dense Feshbach spectrum with more than 40 resonances in a range of 100 G. We use the collision energy tuneability to vary the atom-ion collision energy over several orders of magnitude near one of the resonances and observe the transition from the many-partial-wave to the  $s$ -wave regime, witnessed by a sharp modulation of ion loss. Examining the resonance more closely at energies below  $E_s$ , we find a strong dependence of its amplitude on the collision energy. The behavior can be described by modeling an  $s$ -wave resonance with a beyond threshold quantum recombination model. Additionally, in a nearby magnetic field region, where we detect no resonance at the lowest collision energies, we observe a resonance that appears and peaks at energies around and above  $E_s$ . We find qualitative agreement between this observation and a theoretically modeled  $f$ -wave resonance, underlining the importance of taking higher-partial-wave contributions into account, even at collision energies below  $E_s$ .

## II. EXPERIMENTAL SETUP AND ION LOSS SPECTROSCOPY

We use a hybrid trap setup consisting of a radio-frequency (rf) trap for a single  $^{138}\text{Ba}^+$  ion and a crossed optical dipole trap (xODT) for fermionic  $^6\text{Li}$  atoms [14, 18] (see Fig. 1a). The atoms are spin-polarized in their lowest lying hyperfine state  $|1\rangle_{\text{Li}}$  and cooled to a temperature of  $T_{\text{Li}} \approx 700$  nK. We prepare the ion either in its electronic  $S_{1/2}$  ground or  $D_{3/2}$  metastable excited state. We allow it to interact with the atoms for  $t_{\text{int}}$  and monitor its survival probability  $P_{\text{surv}}$ . During the interaction, we apply an external magnetic field  $B$  and, optionally, an electric displacement field  $\mathcal{E}_{\text{dc}}$ .

The combination of ion and atoms in their respective electronic ground state is chemically stable [10]. Two-body charge exchange collisions, which can occur in other species combinations, are

endothermic. This means that three-body recombination (TBR) is the dominant process for ion loss [14] (Fig. 1b). Measuring the dependence of TBR on  $B$  reveals the atom-ion Feshbach spectrum, a part of which is shown in Fig. 1c (also see Methods and Extended Data). We find a dense spectrum with around 0.5 resonances per Gauss in which some resonances partially overlap. At 321.90(3) G we observe a narrow atom-ion Feshbach resonance with a full width at half maximum (FWHM) of 250(20) mG, clearly distinguishable from the surrounding background.

Conversely, preparation of the ion in the metastable  $D_{3/2}$  state allows for additional inelastic two-body loss processes. At our typical densities, the corresponding ion-loss rate  $\gamma_l$  is at least an order of magnitude higher than that of TBR. As a two-body process,  $\gamma_l$  depends linearly on the atomic density  $\gamma_l \propto n$ , allowing us to probe the profile of the atomic cloud at the position of the ion [19]. As it is based on Langevin collisions,  $\gamma_l$  is not expected to show any dependence on the collision energy [10].

### III. CONTROLLING THE COLLISION ENERGY

The application of a radial displacement field  $\mathcal{E}_{dc}$  during  $t_{int}$  increases the kinetic energy of the ion. This is due to the increase of excess micromotion when the ion is displaced from the rf null [16, 20, 21]. The motion is driven at the rf drive frequency  $\Omega_{rf}$  and, combined with elastic collisions with the atoms, results in a steady-state ion kinetic energy distribution that is non-thermal [22, 23]. In the following, we denote the resulting excess median kinetic energy of the ion as  $\Delta E_{ion}$ . Over the range of displacement fields  $\mathcal{E}_{dc}$  explored here,  $\Delta E_{ion}$  scales quadratically

$$\Delta E_{ion} = \alpha \mathcal{E}_{dc}^2.$$

Using molecular dynamics (MD) simulations (see Methods), we determine the proportionality of  $\alpha = 10(1) \text{ mK}/(\text{V/m})^2$  in our setup. In this way, we can experimentally fine-tune the collision energy by applying  $\mathcal{E}_{dc}$ . Note that the energy scale relevant for collisions is defined in the center of mass (COM) and can be more than twenty times lower than  $\Delta E_{ion}$  due to the mass imbalance of  $m_{Li}/m_{Ba} = 6/138$  and the ultracold temperature of the atomic bath.

The transition to the  $s$ -wave regime, determined by a COM collision energy below  $E_s$ , is reached for  $\Delta E_{s,ion} \approx 195 \mu\text{K} \times \frac{3}{2} k_B$ , for an atomic bath temperature of 700 nK. Our simulations suggest that the ion, sympathetically cooled by the atomic bath, reaches an equilibrium median kinetic energy of  $2.2(2) \mu\text{K} \times \frac{3}{2} k_B$  at stray electric fields compensated to within  $\mathcal{E}_{dc} \approx 3 \text{ mV m}^{-1}$ , our current experimental accuracy. Below  $E_s$  we expect the dimer formation rate  $\Gamma(k)$  for all partial wave channels to depend on the collision energy  $E$  (see Extended Data Fig. 8).

#### IV. FROM THE MANY-PARTIAL-WAVE TO THE $s$ -WAVE REGIME

To probe the density distribution of the Li ensemble  $n(y)$ , we perform ion loss spectroscopy with the ion prepared in the  $D_{3/2}$  state and  $t_{\text{int}} = 40$  ms. We displace the ion vertically from the center of the rf trap by applying  $\mathcal{E}_{\text{dc}}$  and probe  $P_{\text{surv}}$ . This reveals a Gaussian-shaped density distribution  $n(y)$  of width  $\sigma = 8.2(4)$   $\mu\text{m}$ , corresponding to a FWHM of  $19.4(8)$   $\mu\text{m}$  (see Fig. 2). The cloud is offset from the center by  $\mu = 4.9(3)$   $\mu\text{m}$  (see Methods). Interleaved with the density measurement, we prepare the ion in the  $S_{1/2}$  state and probe  $P_{\text{surv}}$  at  $B = 321.90(3)$  G after  $t_{\text{int}} = 200$  ms. This allows us to simultaneously investigate the energy and density dependence of the TBR loss process. At large  $\Delta E_{\text{ion}} > 100$  mK  $\times \frac{3}{2}k_{\text{B}}$  and the corresponding densities we find the TBR loss to be negligible. Reducing the energy to  $\Delta E_{\text{ion}} > 200$   $\mu\text{K} \times \frac{3}{2}k_{\text{B}}$  leads to a decrease of  $P_{\text{surv}}$ . In this regime, the experimental observation agrees with the established classical model, in which  $\gamma_1$  is proportional to  $E^{-3/4}$  and  $n^2$  (see Methods) [16, 17]. The feature, fitted with the classical model, has a FWHM of  $6.9(5)$   $\mu\text{m}$ , narrow compared to the density distribution of the atomic cloud. Further, the TBR loss is centered at zero displacement, albeit being slightly skewed due to the offset of the atomic cloud from the center of the rf trap. Both width and symmetry emphasize the importance of collision energy in the loss process. Continuing to decrease  $\Delta E_{\text{ion}} < \Delta E_{s,\text{ion}}$ , we reveal a sharp modulation of  $P_{\text{surv}}$ , evidencing that the  $321.90(3)$  G resonance begins to dominate the atom-ion interaction. At lowest  $\Delta E_{\text{ion}}$ , the experimental data deviate from the classical model by up to  $21\sigma$ . We associate the deviation for  $\Delta E_{\text{ion}} < \Delta E_{s,\text{ion}}$  with the transition to the quantum regime in which only the lowest partial waves contribute to the loss of the ion; that is, individual Feshbach resonances become pronounced.

#### V. ENERGY DEPENDENCE OF AN $s$ -WAVE RESONANCE

In the context of pronounced collision-energy effects below the  $s$ -wave barrier, we investigate the  $321.90(3)$  G resonance below  $\Delta E_{s,\text{ion}}$  at four distinct collision energies. We measure the Feshbach spectrum in the range  $321.6$  G to  $322.8$  G for  $\Delta E_{\text{ion}} \approx [0, 0.2, 0.45, 0.8] \Delta E_{s,\text{ion}}$  and  $t_{\text{int}} = 200$  ms. In this regime, we observe a strong impact of the collision energy on the Feshbach resonance (see Fig. 3): for higher energies the position of the resonance is shifted towards higher magnetic fields, its amplitude decreases and its width increases. An increase in energy to  $\Delta E_{\text{ion}} \approx 0.8 \Delta E_{s,\text{ion}}$  ( $\approx 7$   $\mu\text{K}$  in the two-body COM) is enough to reduce the amplitude by more than 80%. This is a clear indication of the dominant contribution of  $\Delta E_{\text{ion}}$  to the COM collision energy. We fit the series of resonance scans with skewed Gaussian functions, and derive a linear dependence on  $\Delta E_{\text{ion}}$  of  $2.4(2)$  mG  $\mu\text{K}^{-1}$ .

Additionally, we extract the dependence of the on-resonance loss rate  $\gamma_1$  on  $\Delta E_{\text{ion}}$  and find an exponential decrease with increasing energy. At first, this appears to contradict the threshold scaling laws, which predict an increase of the energy-dependent dimer formation rate  $\Gamma(k)$  for all partial waves. However, the broadening of the resonance illustrates that the width of the collision energy distribution is larger than the natural width of the resonance. In this regime, a broadening of the collision energy distribution with increased  $\Delta E_{\text{ion}}$  counteracts the effect of the threshold scaling law. We compare the scaling of  $\gamma_1$  with the prediction of our quantum recombination model. Our model is based on the two-step mechanism established for narrow resonances in neutral atoms [24–26], but extended to take into account non-thermal energy distributions and beyond threshold effects. This is essential in the case of resonances that are narrow compared to the energy distribution. In the model, a metastable ion-atom dimer state is formed with partial-wave dependent rate  $\Gamma(k)$ , and a secondary collision with another atom at rate  $\Gamma_{\text{inel}}$  causes inelastic recombination (see Methods). Comparing experimental and theoretical results we find the best agreement for an open channel *s*-wave resonance (see inset of Fig. 3) with a weighted sum of squared residuals of  $\chi^2 \approx 14$ . When modeling with a *p*-wave resonance, we find worse agreement with  $\chi^2 \approx 41$ . In contrast, according to our model, resonances attributed to higher partial wave contributions show a qualitatively different behavior. With increasing  $\Delta E_{\text{ion}}$ , they exhibit a significant increase in amplitude in the range below  $\Delta E_{s,\text{ion}}$ , in contradiction to our experimental findings.

## VI. A HIGHER-PARTIAL-WAVE RESONANCE

To elucidate the role of higher partial wave channels experimentally, we perform ion loss spectroscopy in the neighboring range of 319 G to 323 G with  $\Delta E_{\text{ion}} \approx [0, 0.2, 0.45, 0.8, 1.26, 1.81, 3.21] \Delta E_{s,\text{ion}}$  (see Fig. 4). At  $\Delta E_{\text{ion}} = 0$  we observe no significant signal between 320 G and 321.8 G. With increasing energy, a resonance emerges at 320.41(3) G. It peaks in amplitude at  $B = 320.59(3)$  G and  $\Delta E_{\text{ion}} \approx 0.8 \Delta E_{s,\text{ion}}$ . Its position is further shifted to  $B = 321.53(3)$  G at  $\Delta E_{\text{ion}} \approx 1.8 \Delta E_{s,\text{ion}}$  before its signature fades at higher energies. We observe a dependence of the resonance position on  $\Delta E_{\text{ion}}$  of  $4.4(4) \text{ mG } \mu\text{K}^{-1}$ , around twice as large as that of the 321.9 G resonance. Both the peak amplitude at higher  $\Delta E_{\text{ion}}$  and larger shift indicate that the resonance stems from a higher open-channel partial wave (see Methods). Assuming a higher-partial-wave resonance, we compare the experimental results to an *f*-wave resonance that we describe by the quantum recombination model. Choosing the same seven values for  $\Delta E_{\text{ion}}$ , we find that it is very weak at low collision energies but peaks at  $\Delta E_{\text{ion}} = 0.45 \Delta E_{s,\text{ion}}$ . At higher energies, the modeled resonance is further broadened and becomes less pronounced. Based on our experimental findings and their qualitative

agreement with our model, we assume that the observed resonance indeed stems from a higher partial wave channel. Furthermore, we observe a decrease of  $P_{\text{surv}}$  independent of  $B$  when increasing  $\Delta E_{\text{ion}}$ , evidencing the contribution of higher partial-wave channels to background loss. Note that the quantum recombination model, at this point, does not take the effect of the background scattering length into account.

## VII. CONCLUSION AND OUTLOOK

In this Article, we have studied the energy dependence of atom-ion three-body recombination across several orders of magnitude from tens of mK to below  $E_s$  witnessing the transition from the classical to the quantum regime. In the many partial-wave regime ( $\Delta E_{\text{ion}} > 10$  mK) our results can be described by a classical atom-atom-ion recombination model. In the few partial-wave regime, where Feshbach resonances dominate the scattering process, we identified and characterized two individually resolved resonances with different collision energy scaling. While one decreases in amplitude with increasing energy, the other initially increases and peaks at a distinct energy. This implies that the resonances originate in two different open-channel partial waves. Based on the comparison with a beyond-threshold quantum recombination model we conclude that the former is an  $s$ -wave while the latter is a higher partial-wave resonance. Both resonances show a strong dependence on energy below the two-body  $s$ -wave limit, underlining both the importance of reaching low collision energies and the significance of higher partial wave resonances for atom-ion interaction in the ultracold regime.

We expect our findings to advance the understanding of the Li-Ba<sup>+</sup> spectrum and more generally of atom-ion interaction at ultracold temperatures. The experimental assignment of open-channel partial waves enables the theoretical exploration of the role of close-range atom-ion interactions such as second-order spin-orbit coupling or spin-spin interaction. Here the experimental assignment of the open-channel partial wave could allow the direct observation of orbital angular momentum changing collisions. Furthermore, we introduce ion excess kinetic energy as an additional parameter for fast control over atom-ion scattering that can be applied even when rapid changes in the magnetic field are disadvantageous. At a constant magnetic field, the atom-ion system can be tuned to resonance with a higher partial wave resonance by applying an electric displacement field – in principle on a microsecond timescale.

However, we have also shown that at the lowest collision energies currently accessible to hybrid trap setups, non-zero angular momentum resonances still play a significant role. Combining atoms and an ion in an optical dipole trap could allow to avoid any micromotion and reach even lower collision energies [27–29]. This would allow to better distinguish  $s$ - and  $p$ -wave resonances and provide a path

towards the exploration of potentially even more temperature-sensitive many-body complexes. This approach could further allow to experimentally access species combinations of generic mass ratios and extend the single-particle control to the neutral atoms using tightly focussed optical tweezers [30]. Atom-ion systems offer a unique possibility among ultracold systems as the kinetic energy of the atoms and the ion can be tuned individually. However, changing the temperature of the bath comes along with a change in trap laser intensity. The respective impact of bath temperature and trap laser intensity could be disentangled by adiabatic decompression of the atom trap, resulting in different kinetic energy distributions at similar laser intensities. Another interesting property of the bath is its quantum statistics. Admixing the spin-polarized Fermi gas of the experiments presented here with a second spin component could provide insight into the role of Pauli exclusion in atom-atom-ion recombination. This might help to validate whether the two-step model, assuming a resonant two-body and subsequent inelastic loss process, adequately describes atom-atom-ion recombination [31]. In this matter, also broader resonances could be of interest, to test the model in a regime where the collision energy distribution is narrow compared to the linewidth of the resonance.

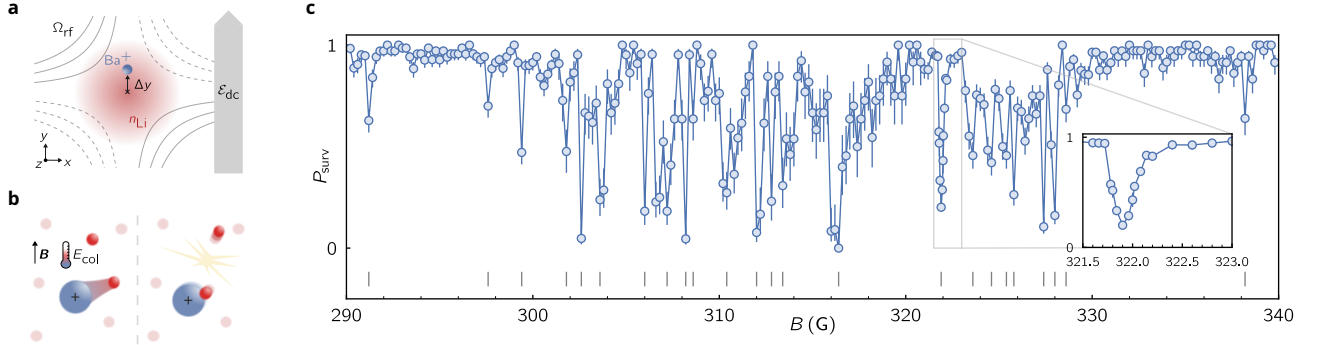


FIG. 1. **Experimental control over atom-ion Feshbach resonances via external fields**

**a** Transverse cut through our hybrid trap setup. A single  $\text{Ba}^+$  ion is confined in a linear radio frequency quadrupole trap (dashed and solid lines) and embedded in a cloud of ultracold, spin-polarized fermionic  $^6\text{Li}$  (red) near degeneracy. An electric field  $\mathcal{E}_{dc}$  (gray arrow) is applied to displace the ion from the center of the rf trap and control the excess kinetic energy of the ion. **b** Illustration of a two-step three-body recombination process: The  $\text{Ba}^+$  ion is interacting with two  $^6\text{Li}$  atoms. Depending on the magnetic field  $B$  and the collision energy, a resonant  $\text{LiBa}^+$  dimer state may be formed. Next, the dimer deexcites to a deeply bound molecular state, releasing its binding energy in the form of kinetic energy of the collision complex. **c** The ion-loss spectrum between 290 and 340 G (blue circles), recorded at lowest collision energy, reveals 24 Feshbach resonances (vertical dashes). Around 322 G (inset) we find a narrow, but pronounced, resonance. The connecting lines serve as a guide to the eye. Errorbars indicate  $1\sigma$  confidence intervals.

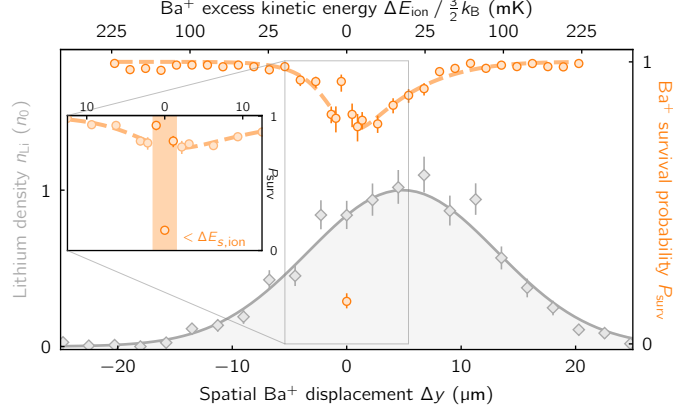


FIG. 2. **Collision energy and density dependence of three-body recombination on an atom-ion Feshbach resonance** We use a single electronically excited  $\text{Ba}^+$  ion in the  $D_{3/2}$  state to probe the *in situ* density of the  $^6\text{Li}$  cloud (gray diamonds) in dependence on its displacement from the center of the rf trap  $\Delta y$ . The density profile is in good agreement with a Gaussian (solid gray line) which is slightly offset from the center of the rf trap. The survival probability of the  $\text{Ba}^+$  ion prepared in the electronic ground state,  $P_{\text{surv}}$ , with the  $B$ -field tuned to resonance (321.9 G) is probed for different excess kinetic energies  $\Delta E_{\text{ion}}$  (orange data points). At higher  $\Delta E_{\text{ion}}$ , the behavior of  $P_{\text{surv}}$  is well described by a classical TBR model (dashed orange line). When tuning to  $\Delta E_{\text{ion}} < 195 \mu\text{K} \times \frac{3}{2}k_B$ , i.e. below the two-body  $s$ -wave limit  $\Delta E_{s,\text{ion}}$  (inset: dark orange markers, shaded region), we observe the emergence of resonant scattering, leading to a slight increase followed by a sharp decrease in  $P_{\text{surv}}$ . At the lowest  $\Delta E_{\text{ion}}$ , we experimentally observe a deviation of  $21\sigma$  from the classical model. The error bars indicate  $1\sigma$  confidence intervals and, where invisible, are smaller than the marker size.

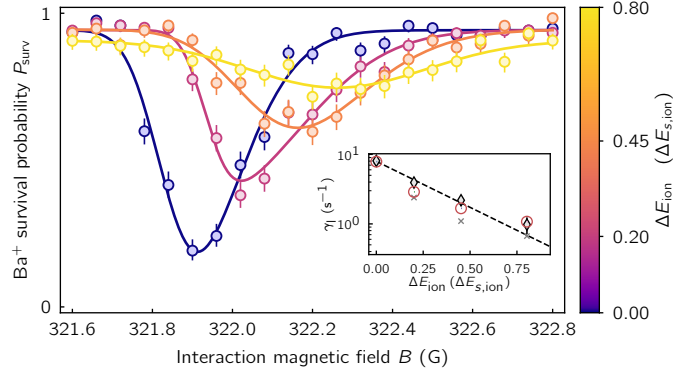


FIG. 3. **Energy dependence of a low partial wave Feshbach resonance**

Ion-loss spectrum around the 321.9 G resonance measured for different  $\text{Ba}^+$  excess kinetic energies. The blue (purple/orange/yellow) data points show  $P_{\text{surv}}$  in dependence on the magnetic field  $B$  for an excess kinetic energy of  $\Delta E_{\text{ion}} \approx 0$  (0.20/0.45/0.80)  $\Delta E_{s,\text{ion}}$ . The temperature of the  $^6\text{Li}$  bath is 700 nK for all  $\Delta E_{\text{ion}}$ . We observe that with increasing  $\Delta E_{\text{ion}}$  the resonance is shifted towards higher magnetic fields, it decreases in amplitude and increases in width. The solid lines are fits with a skewed Gaussian function.

**Inset** The loss rate on resonance  $\gamma_l$  is plotted as a function of  $\Delta E_{\text{ion}}$  (black diamonds). The black dashed line is an exponential fit with a  $1/e$ -energy of  $0.33 \Delta E_{s,\text{ion}}$ . The best quantum recombination model fit to the on-resonant loss rate is achieved for an  $s$ -wave resonance (red circles). For comparison, the best fit for a  $p$ -wave resonance is also shown (gray crosses). The error bars represent  $1\sigma$  confidence intervals and, where invisible, are smaller than the size of the markers.

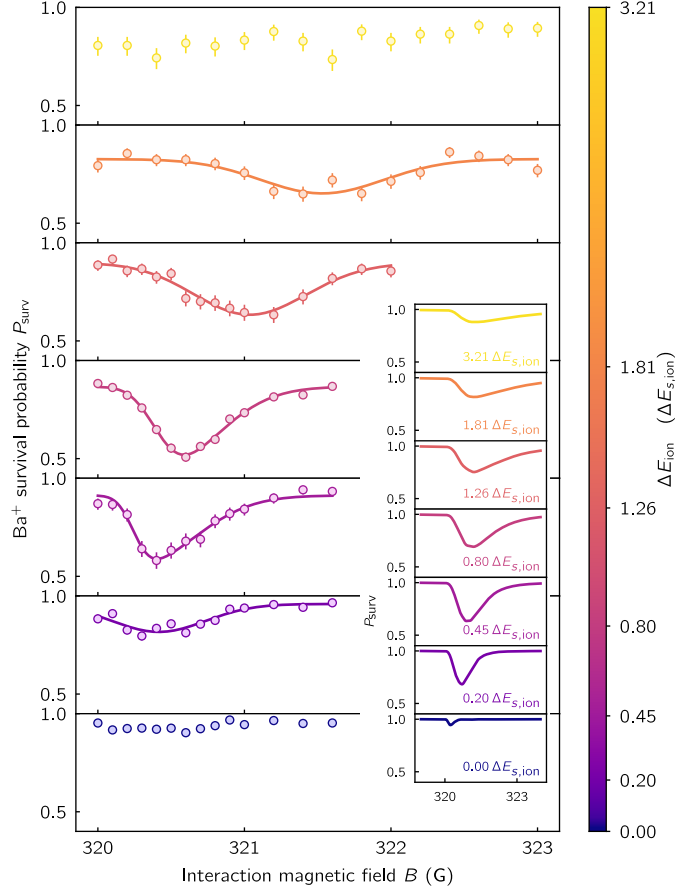


FIG. 4. **Emergence and fading of a higher-partial-wave Feshbach resonance**

Ion-loss spectrum between 320 G and 323 G for increasing excess kinetic energies  $\Delta E_{\text{ion}}$  between 0 and  $3.21 \Delta E_{s,\text{ion}}$  (from bottom to top). Increasing the excess kinetic energy gives rise to a Feshbach resonance that emerges, peaks in amplitude, and disappears in the background at higher collision energies. Along with the effects on the resonance we observe a decrease in  $P_{\text{SURV}}$  on background with increasing collision energy. The solid lines are fits with a skewed Gaussian function. The error bars indicate  $1\sigma$  confidence intervals. **Inset** The inset shows the result of the quantum recombination model. An open-channel  $f$ -wave resonance is modeled for the same seven  $\Delta E_{\text{ion}}$  chosen experimentally. In agreement with our experimental findings we observe a resonance that is weak for lower energies, peaks in amplitude, and vanishes again for higher  $\Delta E_{\text{ion}}$ .

## Appendix A: Methods

### 1. Experimental setup

We operate our rf trap at  $\Omega_{\text{rf}} \approx 2\pi \times 1.43$  MHz creating a time-averaged pseudo-potential with secular frequencies  $\omega_{1,2,3}^{\text{Ba}} = 2\pi \times [66.9, 64.9, 7.2]$  kHz. The generic experimental protocol for ion-loss spectroscopy is as follows: We initially load  $\text{Ba}^+$  ions via ablation loading and, if necessary, isolate a single ion via isotope selective excitation and optical trapping [18, 32]. We then Doppler-cool it and prepare it via optical pumping, either in the electronic ground state  $S_{1/2}$  or the metastable excited  $D_{3/2}$  state. We compensate stray electric fields with an accuracy of  $\mathcal{E}_{\text{stray}} \approx 3 \text{ mV m}^{-1}$ . Then we apply dc control voltages to axially shift the ion out of the center of the rf trap, where we subsequently load a cloud of  ${}^6\text{Li}$  atoms. We evaporatively cool the Li atoms down to temperatures as low as 700 nK and spin-polarize it in its lowest hyperfine state  $|1\rangle_{\text{Li}} = |m_s = -1/2, m_I = 1\rangle$ . Typically, we prepare  $N \approx 1.7 \times 10^4$  atoms at a density of  $n \approx 5 \times 10^{11} \text{ cm}^{-3}$ . The ion is then immersed into the bath of ultracold atoms for an interaction duration  $t_{\text{int}}$ . During  $t_{\text{int}}$ , we apply a magnetic field  $B$  and, optionally, a dc displacement field  $\mathcal{E}_{\text{dc}}$  along the  $y$ -direction to control the collision energy (see below). After  $t_{\text{int}}$ , we interrogate the ion product state via fluorescence detection to determine whether it “survived” the interaction, i.e. it remained cold and in its electronic ground state. We repeat the protocol to derive the ion survival probability  $P_{\text{surv}}$  for a given set of experimental parameters, as well as the related statistical uncertainty based on Wilson score intervals.

### 2. Overlap of ion and atomic cloud

The atomic cloud is trapped in a 1064 nm crossed optical-dipole trap (xODT), consisting of two beams that intersect at an angle of  $14^\circ$  and lie in a plane that forms an angle of  $31^\circ$  with respect to the axial direction of the rf trap. We use piezo mirrors and the AC-Stark shift on the ion to align the trapping beams with the center of the rf trap. During ion-loss spectroscopy experiments, the whole apparatus reaches a steady state, leading to a shift of the xODT position that we observe by absorption imaging. The magnitude of this shift is consistent with the offset observed in Fig. 2.

### 3. Ion state preparation and readout

The ion is initially Doppler cooled using the  $S_{1/2}$  to  $P_{1/2}$  transition, in combination with a repumping laser from the  $D_{3/2}$  state. To prepare the ion in the  $S_{1/2}$  ( $D_{3/2}$ ) state, we switch off the cooling (repumping) laser 50 ms before the end of the Doppler cooling phase. At this point we do

not spin polarize the ion in a specific Zeeman state. In addition to Doppler cooling, limited to  $\approx 360 \mu\text{K}$ , the ion is sympathetically cooled in the ultracold atomic bath to lower temperatures. From simulations, we obtain a lower limit for the median ion kinetic energy of  $2.2 \mu\text{K} \times k_B$ . This is consistent with our observation of a broadening of the 321.9G resonance, when we increase the temperature of the atomic bath from 700 nK to  $2.75 \mu\text{K}$ . From the experimental results presented in this article, we also conclude an upper limit of  $\approx 30 \mu\text{K} \times k_B$ , as increasing  $\Delta E_{\text{ion}}$  by this amount, gives rise to significant changes in the resonance shape. After the interaction, we interrogate the ion product state based on fluorescence detection of the ion. First, we only switch on a near-detuned cooling laser and the repumping laser from the  $D_{3/2}$  state, then we successively add a far-detuned cooling laser and a repumping laser from the  $D_{5/2}$  state. In this way, we distinguish between a direct detection (“survival”), a heated ion (“hot”), an ion in the metastable  $D_{5/2}$  state and ion loss from the trap. In this article, we refer to the probability of a survival event as  $P_{\text{surv}}$  and, for the sake of readability, define any signature of an inelastic process as loss, i.e.  $P_{\text{loss}} = 1 - P_{\text{surv}}$ . We performed independent measurements to verify that  $P_{\text{surv}}$  follows an exponential decay with  $t_{\text{int}}$  for both the inelastic two-body loss and TBR. This allows us to extract the loss rate  $\gamma_1 = -\frac{\ln P_{\text{surv}}}{t_{\text{int}}}$ . Note that this is different from the case of neutral-atom experiments, in which the density dependence of different loss processes leads to different superexponential scalings. The experimental data presented in Fig. 2 and 3 was recorded in a fully interleaved fashion. The spectra presented in Fig. 4 were partially recorded in individual runs.

#### 4. Ion loss spectrum

We calibrate the magnetic field by performing rf-spectroscopy on the Li  $|1\rangle \rightarrow |2\rangle$  hyperfine transition. Long-term measurements reveal that the field is stable within  $\sigma_{B,\text{stat}} = 24 \text{mG}$  over the course of 12 hours. The systematic uncertainty of the calibration for the entire range of B is  $\sigma_{B,\text{sys}} = 80 \text{mG}$ . To record the spectrum presented in Fig. 5 we performed ion loss spectroscopy with  $\Delta E_{\text{ion}} = 0$ . The range of 100 G was sampled with individual scans of 10 G with step size of 200 mG. Interleaved with this we sample the 321.90(3) G resonance with a finer step size to rule out magnetic field drifts or loss of contrast due to a decrease in overlap between the ion and the atoms. We classify individual resonances as local minima that are separated from the next local minimum by a barrier of at least  $3\sigma$  height. In this way, we identify 49 resonances of different widths and amplitudes in the range of 240 G to 340 G, on average  $0.580(7) \text{G}^{-1}$ . In the spectra of lanthanides that exhibit a high resonance density (e.g.  $3.4 \text{G}^{-1}$  for  $^{168}\text{Er}$  at comparable collision energy [5]), a statistical analysis revealed properties of chaotic scattering. We follow the same analysis of the

number variance  $\Sigma^2$  and normalized nearest neighbor spacing  $s$  as presented in [5, 33, 34] and show that both are in good agreement with a Poissonian (i.e. non-interacting) distribution of resonances (see Fig. 6). Both  $\Sigma^2$  and  $P(s)$  deviate significantly from a Wigner-Dyson distribution that would be expected for chaotic scattering. We conclude that within the resolution of our experiment, we do not observe any signature of chaotic scattering.

## 5. Tuning the ion excess kinetic energy

We run MD simulations to find the kinetic energy scaling of the ion with respect to the applied displacement field  $\mathcal{E}_{\text{dc}}$  [35, 36]. The simulations are performed in three spatial dimensions and include the radial rf fields, as well as the long-range attractive  $C_4$  and short-range repulsive  $C_6$  atom-ion interaction potential. At this point, we neglect the contribution of axial or phase micromotion. We simulate a large number of collisions between the ion and a single atom. For each collision, the atom is initialized on a sphere with radius  $r_{\text{init}}$  around the ion. The atomic kinetic energies are sampled from a thermal distribution. The ion is initially at rest and, over time and averaging over many trajectories, reaches a steady-state median kinetic energy. We perform these simulations for different displacement fields  $\mathcal{E}_{\text{dc}}$  and obtain the scaling factor

$$\alpha_{\text{sim}} \approx 10(1) \text{ mK}/(\text{V/m})^2$$

corresponding to  $\approx 420(40) \mu\text{K}/(\text{V/m})^2$  in the two-body COM (see Fig. 7).

Note that we use the median kinetic energy, as the characteristic power law distribution of ion kinetic energies makes the mean an unreliable statistical measure due to the strong influence of high-energy outliers.

Independently, we can estimate  $\alpha$  for the isolated ion based on the rf trap parameters [20] as

$$\alpha_{\text{theo},i} = \frac{4}{m} \left( \frac{eq_i}{(2a_i + q_i^2)\Omega_{\text{rf}}} \right)^2, \quad (\text{A1})$$

with  $i$  indicating the spatial direction, the trap parameters  $a_i$  and  $q_i$ , the mass of the ion  $m$ , the elementary charge  $e$  and the angular drive frequency of the rf trap  $\Omega_{\text{rf}}$ . For our trap configuration and displacement in the  $y$ -direction we obtain

$$\alpha_{\text{theo},y} \approx 16.4(10) \text{ mK}/(\text{V/m})^2.$$

We thus find a 60% larger value compared to simulating the full atom-ion dynamics, likely due to effects of atom-ion collisions as well as applying the median instead of the mean to the energy distribution.

Another feature of the kinetic energy distribution of the ion is a strong anisotropy (see inset of Fig. 7). As  $\mathcal{E}_{\text{dc}}$  is applied in the radial direction, the kinetic energy distribution in the radial plane has a strong nonthermal component. In an ideal trap, the ion is only heated axially by collisional redistribution of the radial kinetic energy. This results in a kinetic energy distribution much closer to that of a thermal ensemble. We use simulated 3D ion velocity distributions when modeling the behavior of resonances with the quantum recombination model.

## 6. Additional confidence tests

To ensure that our observations can be attributed to collision-energy effects, in addition to the evidence already presented in the main text, we perform the following confidence tests: First, we use a different method to tune the collision energy. When increasing the atomic bath temperature from 700 nK to 2.8  $\mu\text{K}$ , we observe a broadening of the 321.9 G resonance that is in agreement with predictions of the quantum recombination model. Other effects, such as an overall increase in loss, likely associated with the increase in the intensity of the xODT beam, make it difficult to directly compare this method with the ion excess kinetic energy method. The impact of the trap light, for example light-assisted losses and an AC-Stark shift of the resonance, has also been reported elsewhere [34] and is currently under investigation for Li-Ba<sup>+</sup>. Second, we increase the radial confinement provided by the rf fields by a factor of two. At  $\Delta E_{\text{ion}} = 0$ , we do not find any significant differences in the shape, position, or amplitude of the 321.9 G resonance. From this we conclude that trap-induced bound states, as reported in [37, 38], do not significantly affect the resonance. Increasing  $\Delta E_{\text{ion}}$  at higher confinement, we find that applying approximately twice the displacement field results in a similar shift and decrease in amplitude as presented in Fig. 3. This is in agreement with Eq. A1.

## 7. Classical description of three-body recombination loss

In an independent measurement we confirm that, on a Feshbach resonance, the loss rate  $\gamma_1$  is proportional to  $n^2$  [14]. It was further shown in experiment and theory that in the classical regime the atom-ion TBR rate scales with  $E^{-3/4}$  [16, 17]. To model the energy at which the survival probability no longer follows a classical scaling, we introduce a minimum energy  $E_0$ . The loss rate is thus  $\gamma_1 = k_3 n^2 (E_0 + \Delta E_{\text{ion}})^{-3/4}$ . We find a good fit with our experimental data taken at  $\Delta E_{\text{ion}} > \Delta E_{s,\text{ion}}$  for  $E_0 = 4.5(8) \text{ mK} \times \frac{3}{2} k_{\text{B}}$  (corresponding to 190(30)  $\mu\text{K}$  in the two-body COM frame) and a  $k_3$ -parameter of  $2.31(23) \times 10^{-23} \text{ cm}^{-6} \text{ s}^{-1}$  at 10 mK.

## 8. Quantum recombination model

The three-body cross section is given by

$$\sigma(k) = \frac{\pi}{k^2} \frac{\Gamma(k)\mathcal{K}(k)n}{(\varepsilon - \varepsilon_{\text{res}})^2 + (\Gamma(k) + \mathcal{K}(k)n)^2/4}$$

where  $\Gamma(k)$  is the resonance width,  $\mathcal{K}(k)$  being the rate constant describing the inelastic atom-molecule collision,  $n$  the atomic gas density,  $\varepsilon_{\text{res}} = \delta\mu(B - B_{\text{res}})$  the resonance position, and  $k$  is the wavevector corresponding to the collision energy in the three-body relative frame  $\varepsilon$ .  $\Gamma(k)$  can be separated into a product of the energy-independent short-range coupling  $\Gamma_m$  and the quantum defect function  $C^{-2}(k)$  which provides the threshold behavior at low energy scaling  $C^{-2}(k) \propto k^{2\ell+1}$  and approaches unity at large energies, providing a direct way to describe resonances far above the Wigner threshold regime. For the inelastic rate constant  $\mathcal{K}(k)$  we employ the quantum defect model, assuming that the collision between the atom and the two-body complex is universal, i.e. the probability of reaction at short range approaches unity. The resulting energy-dependent reaction rate does not depend on any free parameters, although this assumption can be relaxed [39, 40]. The rates  $\Gamma(k)$  and  $\Gamma_{\text{inel}}(k) = \mathcal{K}(k)n$  have to be averaged over the proper energy distribution, taking into account that the sample is non-thermal (the ion and the atoms follow different energy distributions and we are interested in the energy in the three-body relative frame). The model has multiple free parameters: the resonance is described by the bare width  $\Gamma(k)$ , the differential magnetic moment  $\delta\mu$ ,  $C^{-2}(k)$  depends on the background scattering length of the open channel and its partial wave, and the assumptions about the energy distribution of the ion have to be made; additionally, it neglects scattering in other partial waves, spin-orbit coupling effects as well as Stark shifts from the lasers and the rf field.

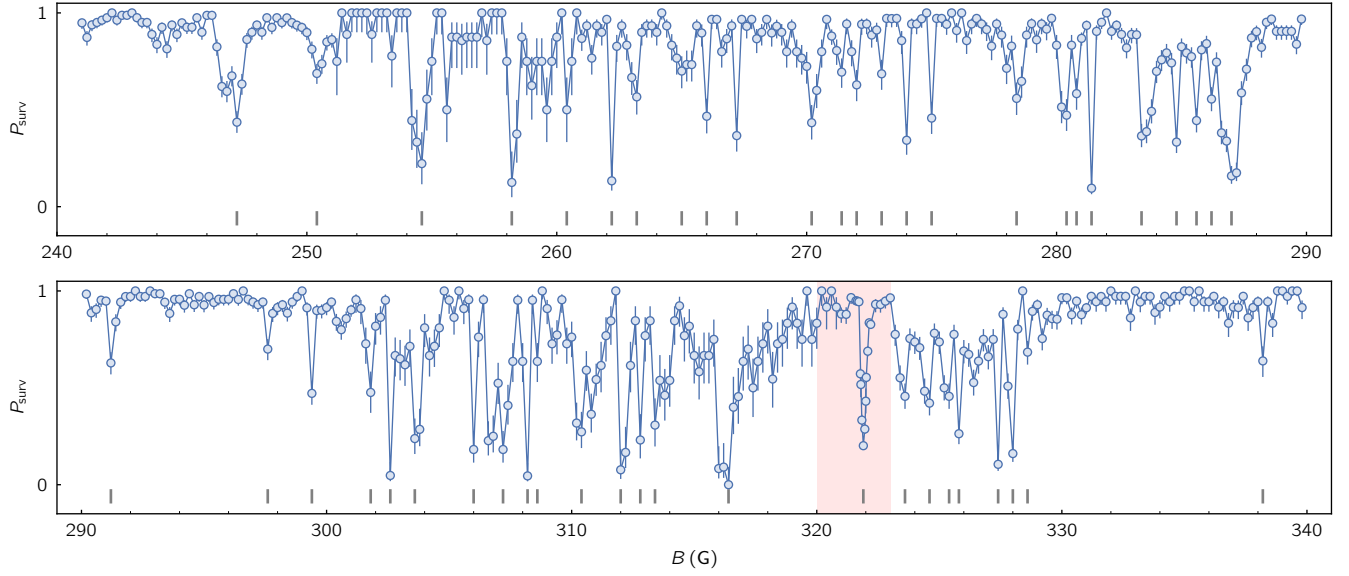


FIG. 5. **Ion loss spectrum for  ${}^6\text{Li}$  prepared in  $\text{S}_{1/2}(m_s = -1/2, m_I = 1)$ :** The ion survival probability  $P_{\text{surv}}$  is plotted in dependence on the magnetic field  $B$ . With the ion excess kinetic energy tuned to  $\Delta E_{\text{ion}} = 0$ , we find 49 resonances (vertical dashes) between 240 G and 340 G. The red-shaded region, including the narrow resonance at 321.9 G, is investigated for energy dependence in this paper. The error bars indicate  $1\sigma$  confidence intervals.

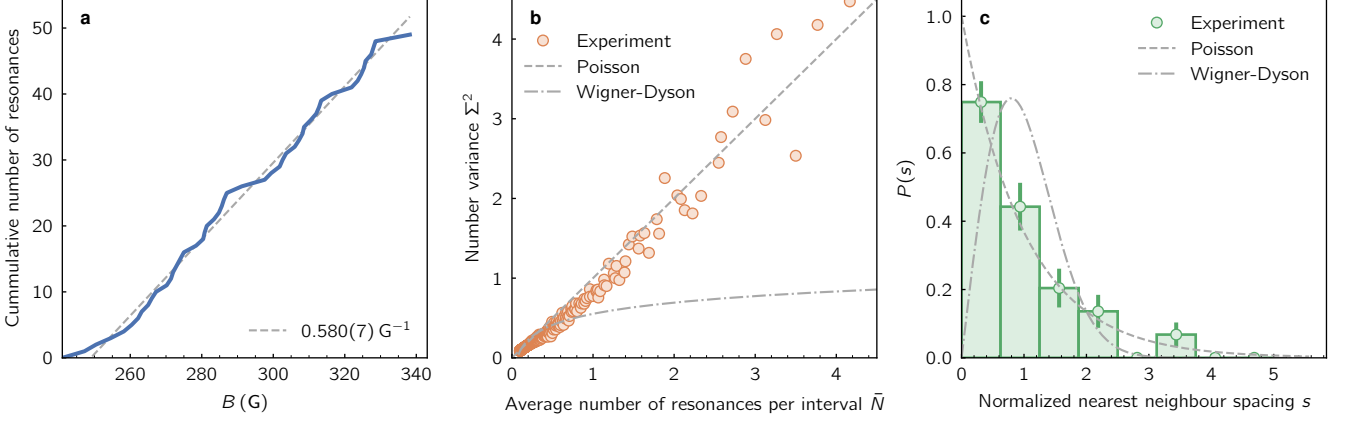


FIG. 6. **Statistical analysis of the resonance spectrum:** **a** We plot the cumulative number of resonances as a function of the applied field  $B$  (blue line). We observe a linear behavior and use a fit to determine the average resonance density  $\bar{\rho} = 0.580(7) \text{ G}^{-1}$ . **b** The variance  $\Sigma^2$  of the number of resonances in an interval is plotted as a function of the average number of resonances in that interval  $\bar{N}$ . The experimental data (blue markers) are consistent with the scaling of Poisson-distributed resonances (dashed line) and deviate significantly from a Wigner-Dyson distribution. **c** The probability distribution of the normalized nearest-neighbor spacing  $s = \bar{\rho} \delta B$  also shows consistency between the resonance positions observed experimentally (green markers) and a Poisson-distributed sample (dashed line). For comparison, a Wigner-Dyson distribution, featuring the characteristic anti-bunching, is also plotted (dash-dotted line).

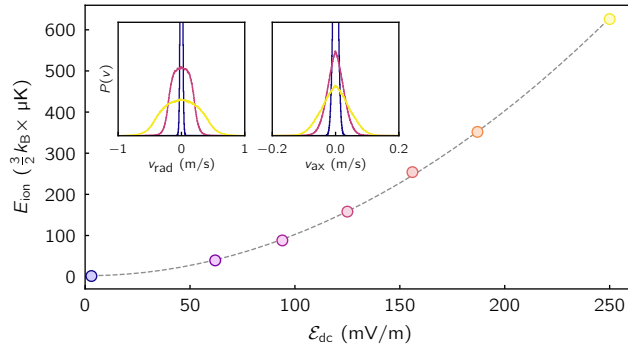


FIG. 7. **Ion kinetic energy scaling:** The lab frame median ion kinetic energy  $E_{\text{ion}}$ , based on our simulations, is shown in dependence on the applied displacement field  $\mathcal{E}_{\text{dc}}$  (circles). The data are fitted with a quadratic function to obtain  $\alpha_{\text{sim}}$  (gray dashed line). The two insets show the radial and axial velocity distribution for  $3(125/250) \text{ mV m}^{-1}$  (blue/purple/yellow line). Both plots are capped vertically to improve the visibility of the broadened distributions at higher  $\mathcal{E}_{\text{dc}}$ .

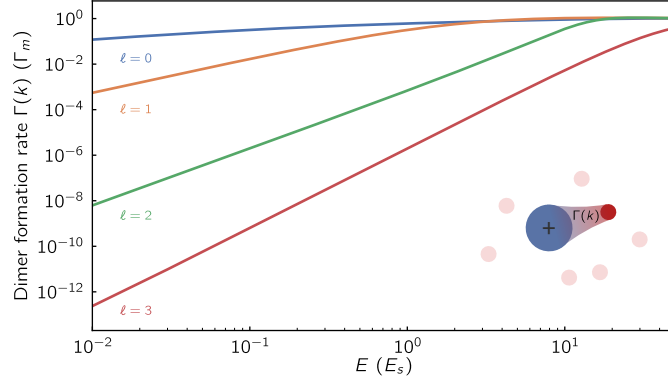


FIG. 8. **Energy scaling of the dimer formation rate:** The theoretical dimer formation rate  $\Gamma$  is plotted in dependence on the collision energy for the lowest four partial waves. At low energies, all partial waves exhibit the characteristic scaling of  $E^{\ell+\frac{1}{2}}$ , while reaching unity at distinct finite energies.

## Appendix B: Acknowledgements

This project has received funding from the European Research Council (ERC) under the European Union’s Horizon 2020 research and innovation programme (grant number 648330), the Deutsche Forschungsgemeinschaft (DFG, grant number SCHA 973/9-1-3017959) and the Georg H. Endress Foundation. F.T., J.S., D.v.S. and T.S. acknowledge financial support from the DFG via the RTG DYNCAM 2717. W.W. acknowledges financial support from the QUSTEC programme, funded by the European Union’s Horizon 2020 research and innovation programme under the Marie Skłodowska-Curie (grant number 847471). P.W. gratefully acknowledges financial support from the Studienstiftung des deutschen Volkes. K.J. was supported by the Polish National Agency for Academic Exchange (NAWA) via the Polish Returns 2019 programme. T.W. and T.S. acknowledge financial support from the Georg H. Endress foundation. We thank Ulrich Warring, Dietrich Leibfried, Jesús Pérez-Ríos and Michał Tomza for fruitful discussion.

## Appendix C: Authorship

F.T. and J.S. carried out the experiments and analyzed the data with support from T.W. and under supervision of T.S. F.T., J.S., D.v.S., W.W. and P.W. built the experiment. F.T. performed the MD simulations. K.J. performed the theoretical calculations. F.T. and T.S. prepared the manuscript, with contributions from all authors. All authors participated in the interpretation of the data.

## Appendix D: Data availability

The data presented in this paper is available from the corresponding author upon request.

## Appendix E: Code availability

The `julia` code used to simulate the ion dynamics in the atomic bath is available upon request. The code used to analyze the raw data is available upon request. The code used to simulate the quantum recombination model is available upon request.

- 
- [1] J. Dalibard, Collisional dynamics of ultra-cold atomic gases, in *Bose-Einstein Condensation in Atomic Gases*, Proceedings of the International School of Physics "Enrico Fermi" (1999) pp. 321–349.

- [2] C. Chin, R. Grimm, P. Julienne, and E. Tiesinga, Feshbach resonances in ultracold gases, *Reviews of Modern Physics* **82**, 1225 (2010).
- [3] I. Bloch, J. Dalibard, and W. Zwerger, Many-body physics with ultracold gases, *Reviews of Modern Physics* **80**, 885 (2008).
- [4] B. DeMarco, J. L. Bohn, J. P. Burke, M. Holland, and D. S. Jin, Measurement of p -Wave Threshold Law Using Evaporatively Cooled Fermionic Atoms, *Physical Review Letters* **82**, 4208 (1999).
- [5] T. Maier, H. Kadau, M. Schmitt, M. Wenzel, I. Ferrier-Barbut, T. Pfau, A. Frisch, S. Baier, K. Aikawa, L. Chomaz, M. J. Mark, F. Ferlaino, C. Makrides, E. Tiesinga, A. Petrov, and S. Kotochigova, Emergence of Chaotic Scattering in Ultracold Er and Dy, *Physical Review X* **5**, 041029 (2015).
- [6] J. J. Park, Y.-K. Lu, A. O. Jamison, T. V. Tscherbul, and W. Ketterle, A Feshbach resonance in collisions between triplet ground-state molecules, *Nature* **614**, 54 (2023).
- [7] B. Margulis, K. P. Horn, D. M. Reich, M. Upadhyay, N. Kahn, A. Christianen, A. Van Der Avoird, G. C. Groenenboom, M. Meuwly, C. P. Koch, and E. Narevicius, Tomography of Feshbach resonance states, *Science* **380**, 77 (2023).
- [8] A. B. Henson, S. Gersten, Y. Shagam, J. Narevicius, and E. Narevicius, Observation of Resonances in Penning Ionization Reactions at Sub-Kelvin Temperatures in Merged Beams, *Science* **338**, 234 (2012).
- [9] A. Härter and J. Hecker Denschlag, Cold atom–ion experiments in hybrid traps, *Contemporary Physics* **55**, 33 (2014).
- [10] M. Tomza, K. Jachymski, R. Gerritsma, A. Negretti, T. Calarco, Z. Idziaszek, and P. S. Julienne, Cold hybrid ion-atom systems, *Reviews of Modern Physics* **91**, 035001 (2019).
- [11] M. Deiß, S. Willitsch, and J. Hecker Denschlag, Cold trapped molecular ions and hybrid platforms for ions and neutral particles, *Nature Physics* **20**, 713 (2024).
- [12] T. Karman, M. Tomza, and J. Pérez-Ríos, Ultracold chemistry as a testbed for few-body physics, *Nature Physics* **20**, 722 (2024).
- [13] T. Feldker, H. FÜRST, H. Hirzler, N. V. Ewald, M. Mazzanti, D. Wiater, M. Tomza, and R. Gerritsma, Buffer gas cooling of a trapped ion to the quantum regime, *Nature Physics* **16**, 413 (2020).
- [14] P. Weckesser, F. Thielemann, D. Wiater, A. Wojciechowska, L. Karpa, K. Jachymski, M. Tomza, T. Walker, and T. Schaetz, Observation of Feshbach resonances between a single ion and ultracold atoms, *Nature* **600**, 429 (2021).
- [15] T. V. Tscherbul, P. Brumer, and A. A. Buchachenko, Spin-Orbit Interactions and Quantum Spin Dynamics in Cold Ion-Atom Collisions, *Physical Review Letters* **117**, 143201 (2016).

- [16] A. Krüchow, A. Mohammadi, A. Härter, J. H. Denschlag, J. Pérez-Ríos, and C. H. Greene, Energy Scaling of Cold Atom-Atom-Ion Three-Body Recombination, *Physical Review Letters* **116**, 193201 (2016).
- [17] J. Pérez-Ríos and C. H. Greene, Communication: Classical threshold law for ion-neutral-neutral three-body recombination, *The Journal of Chemical Physics* **143**, 041105 (2015).
- [18] P. Weckesser, F. Thielemann, D. Hoenig, A. Lambrecht, L. Karpa, and T. Schaetz, Trapping, shaping, and isolating of an ion Coulomb crystal via state-selective optical potentials, *Physical Review A* **103**, 013112 (2021).
- [19] J. Joger, H. FÜRST, N. Ewald, T. Feldker, M. Tomza, and R. Gerritsma, Observation of collisions between cold Li atoms and Yb + ions, *Physical Review A* **96**, 030703 (2017).
- [20] D. J. Berkeland, J. D. Miller, J. C. Bergquist, W. M. Itano, and D. J. Wineland, Minimization of ion micromotion in a Paul trap, *Journal of Applied Physics* **83**, 5025 (1998).
- [21] M. Cetina, A. T. Grier, and V. Vuletić, Micromotion-Induced Limit to Atom-Ion Sympathetic Cooling in Paul Traps, *Physical Review Letters* **109**, 253201 (2012).
- [22] M. Pinkas, Z. Meir, T. Sikorsky, R. Ben-Shlomi, N. Akerman, and R. Ozeri, Effect of ion-trap parameters on energy distributions of ultra-cold atom-ion mixtures, *New Journal of Physics* **22**, 013047 (2020).
- [23] B. Höltkemeier, P. Weckesser, H. López-Carrera, and M. Weidemüller, Buffer-Gas Cooling of a Single Ion in a Multipole Radio Frequency Trap Beyond the Critical Mass Ratio, *Physical Review Letters* **116**, 233003 (2016).
- [24] Q. Beaufils, A. Crubellier, T. Zanon, B. Laburthe-Tolra, E. Maréchal, L. Vernac, and O. Gorceix, Feshbach resonance in d -wave collisions, *Physical Review A* **79**, 032706 (2009).
- [25] L. Fouché, A. Boissé, G. Berthet, S. Lepoutre, A. Simoni, and T. Bourdel, Quantitative analysis of losses close to a d -wave open-channel Feshbach resonance in K 39, *Physical Review A* **99**, 022701 (2019).
- [26] J. Li, J. Liu, L. Luo, and B. Gao, Three-Body Recombination near a Narrow Feshbach Resonance in Li 6, *Physical Review Letters* **120**, 193402 (2018).
- [27] T. Schaetz, Trapping ions and atoms optically, *Journal of Physics B: Atomic, Molecular and Optical Physics* **50**, 102001 (2017).
- [28] A. Lambrecht, J. Schmidt, P. Weckesser, M. Debatin, L. Karpa, and T. Schaetz, Long lifetimes and effective isolation of ions in optical and electrostatic traps, *Nature Photonics* **11**, 704 (2017).
- [29] J. Schmidt, P. Weckesser, F. Thielemann, T. Schaetz, and L. Karpa, Optical Traps for Sympathetic Cooling of Ions with Ultracold Neutral Atoms, *Physical Review Letters* **124**, 053402 (2020).

- [30] M. Endres, H. Bernien, A. Keesling, H. Levine, E. R. Anschuetz, A. Krajenbrink, C. Senko, V. Vuletic, M. Greiner, and M. D. Lukin, Atom-by-atom assembly of defect-free one-dimensional cold atom arrays, *Science* **354**, 1024 (2016).
- [31] M. Lecomte, A. Journeaux, L. Renaud, J. Dalibard, and R. Lopes, Loss features in ultracold  $^{162}\text{Dy}$  gases: Two- versus three-body processes, *Physical Review A* **109**, 023319 (2024).
- [32] J. Schmidt, D. Hönig, P. Weckesser, F. Thielemann, T. Schaetz, and L. Karpa, Mass-selective removal of ions from Paul traps using parametric excitation, *Applied Physics B* **126**, 176 (2020).
- [33] A. Frisch, M. Mark, K. Aikawa, F. Ferlaino, J. L. Bohn, C. Makrides, A. Petrov, and S. Kotochigova, Quantum chaos in ultracold collisions of gas-phase erbium atoms, *Nature* **507**, 475 (2014).
- [34] V. A. Khlebnikov, D. A. Pershin, V. V. Tsyganok, E. T. Davletov, I. S. Cojocaru, E. S. Fedorova, A. A. Buchachenko, and A. V. Akimov, Random to Chaotic Statistic Transformation in Low-Field Fano-Feshbach Resonances of Cold Thulium Atoms, *Physical Review Letters* **123**, 213402 (2019).
- [35] H. A. FÜRST, N. V. Ewald, T. Secker, J. Joger, T. Feldker, and R. Gerritsma, Prospects of reaching the quantum regime in Li–Yb<sup>+</sup> mixtures, *Journal of Physics B: Atomic, Molecular and Optical Physics* **51**, 195001 (2018).
- [36] E. Trimby, H. Hirzler, H. FÜRST, A. Safavi-Naini, R. Gerritsma, and R. S. Lous, Buffer gas cooling of ions in radio-frequency traps using ultracold atoms, *New Journal of Physics* **24**, 035004 (2022).
- [37] H. Hirzler, E. Trimby, R. Gerritsma, A. Safavi-Naini, and J. Pérez-Ríos, Trap-Assisted Complexes in Cold Atom-Ion Collisions, *Physical Review Letters* **130**, 143003 (2023).
- [38] M. Pinkas, O. Katz, J. Wengrowicz, N. Akerman, and R. Ozeri, Trap-assisted formation of atom-ion bound states, *Nature Physics* **19**, 1573 (2023).
- [39] B. Gao, Quantum Langevin model for exoergic ion-molecule reactions and inelastic processes, *Physical Review A* **83**, 062712 (2011).
- [40] K. Jachymski, M. Krych, P. S. Julienne, and Z. Idziaszek, Quantum Theory of Reactive Collisions for  $1/r^n$  Potentials, *Physical Review Letters* **110**, 213202 (2013).